GRANT NO: DAMD17-93-J-3009

TITLE: DIGITAL MAMMOGRAPHY WITH STORAGE PHOSPHORS

PRINCIPAL INVESTIGATOR: Chris C. Shaw, Ph.D.

CONTRACTING ORGANIZATION: University of Pittsburgh
Department of Radiology
A441 Scaife Hall
Pittsburgh, Pennsylvania 15261

REPORT DATE: December 31, 1993

TYPE OF REPORT: Annual Report

PREPARED FOR: U.S. Army Medical Research and
Development Command, Fort Detrick
Frederick, Maryland 21702-5012

DISTRIBUTION STATEMENT: Approved for public release;
distribution unlimited

REPORT DOCUMENTATION PAGE

Form Approved
OMB No 0704-0188

1. AGENCY USE ONLY (Leave blank)	2. REPORT DATE	3. REPORT TYPE AND DATES COVERED
	December 31, 1993	Annual Report (12/1/92 - 11/30/93)

4. TITLE AND SUBTITLE
Digital Mammography with Storage Phosphors

5. FUNDING NUMBERS
Grant No.
DAMD17-93-J-3009

6. AUTHOR(S)
Chris C. Shaw, Ph.D.

7. PERFORMING ORGANIZATION NAME(S) AND ADDRESS(ES)
University of Pittsburgh
Department of Radiology
A441 Scaife Hall
Pittsburgh, Pennsylvania 15261

8. PERFORMING ORGANIZATION REPORT NUMBER

9. SPONSORING/MONITORING AGENCY NAME(S) AND ADDRESS(ES)
U.S. Army Medical Research & Development Command
Fort Detrick
Frederick, Maryland 21702-5012

10. SPONSORING/MONITORING AGENCY REPORT NUMBER

11. SUPPLEMENTARY NOTES

All requests for the microfilms referenced in the subject annual report should be made to:

Chris C. Shaw, Ph.D.
Department of Radiology
A441 Scaife Hall
University of Pittsburgh
Pittsburgh, Pennsylvania 15261

13. ABSTRACT *(Maximum 200 words)*

In the first year of grant period, we have completed the following tasks:

1. We have improved the spatial resolution capability of our storage phosphor image reader by using a high resolution phosphor and by reducing the laser spot size from 120 μm to 50 μm.
2. We have compared the spatial resolution capability of the improved system with those of the unmodified system and a Min-R screen-film combination.
3. We have investigated the method of constructing phantoms for the comparison study.
4. We have developed and tested compression algorithms for mammographic images.

The completion of the above mentioned tasks has resulted in an improved storage phosphor imaging system for mammographic applications. We have demonstrated with phantom images that the quality of the storage phosphor images, obtained with the improved imaging system, is comparable to that of the screen-film images acquired with a clinical mammographic unit at our institution. With the completion of the above tasks, we are largely prepared to start acquiring phantom images for the ROC studies.

14. SUBJECT TERMS	15. NUMBER OF PAGES
Digital Radiography, Mammography, Breast Imaging, Computed Radiography, Storage Phosphor, Breast Cancer RAD VI	16. PRICE CODE

17. SECURITY CLASSIFICATION OF REPORT	18. SECURITY CLASSIFICATION OF THIS PAGE	19. SECURITY CLASSIFICATION OF ABSTRACT	20. LIMITATION OF ABSTRACT
Unclassified	Unclassified	Unclassified	Unlimited

FOREWORD

Opinions, interpretations, conclusions and recommendations are those of the author and are not necessarily endorsed by the U.S. Army.

(x) Where copyrighted material is quoted, permission has been obtained to use such material.

(X) Where material from documents designated for limited distribution is quoted, permission has been obtained to use the material.

(X) Citations of commercial organizations and trade names in this report do not constitute an official Department of the Army endorsement or approval of the products or services of these organizations.

(N.A.) In conducting research using animals, the investigator(s) adhered to the "Guide for the Care and Use of Laboratory Animals," prepared by the Committee on Care and Use of Laboratory Animals of the Institute of Laboratory Animal Resources, National Research Council (NIH Publication No. 86-23, Revised 1985).

(N.A.) For the protection of human subjects, the investigator(s) have adhered to policies of applicable Federal Law 45 CFR 46.

(N.A.) In conducting research utilizing recombinant DNA technology, the investigator(s) adhered to current guidelines promulgated by the National Institutes of Health.

Chris C. Shaw

PI Signature

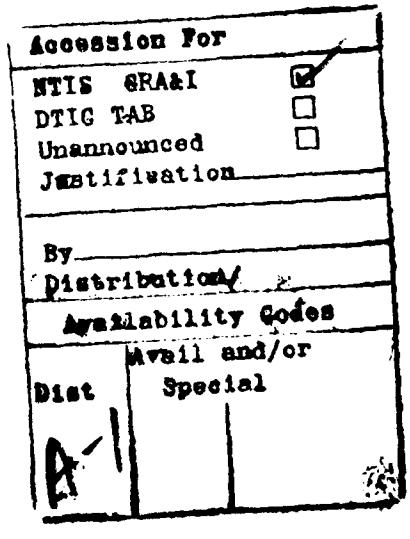

TABLE OF CONTENTS

EXPERIMENTAL METHODS

System Modifications

Figure 1 shows a schematic diagram of the laser scanning optics used in our experimental image reader. The collimated beam from an argon laser unit passes through a lens A and focuses at the acoustic optical modulator (AOM). The divergent output is collimated again by lens C, reflected by mirror D and focused again by a microscopic objective lens F. An aperture E is used to block the zero order peak and select the first order peak of the AOM output. The latter has an intensity adjustable through digital control of the AOM. The output of the lens F is collimated into a widened beam by lens G (beam expander) which is reflected by the mirror H and deflected by the digitally controlled galvanometer mirror I. The deflected beam passes through an F-theta or laser scan lens J and focuses on the image plane K.

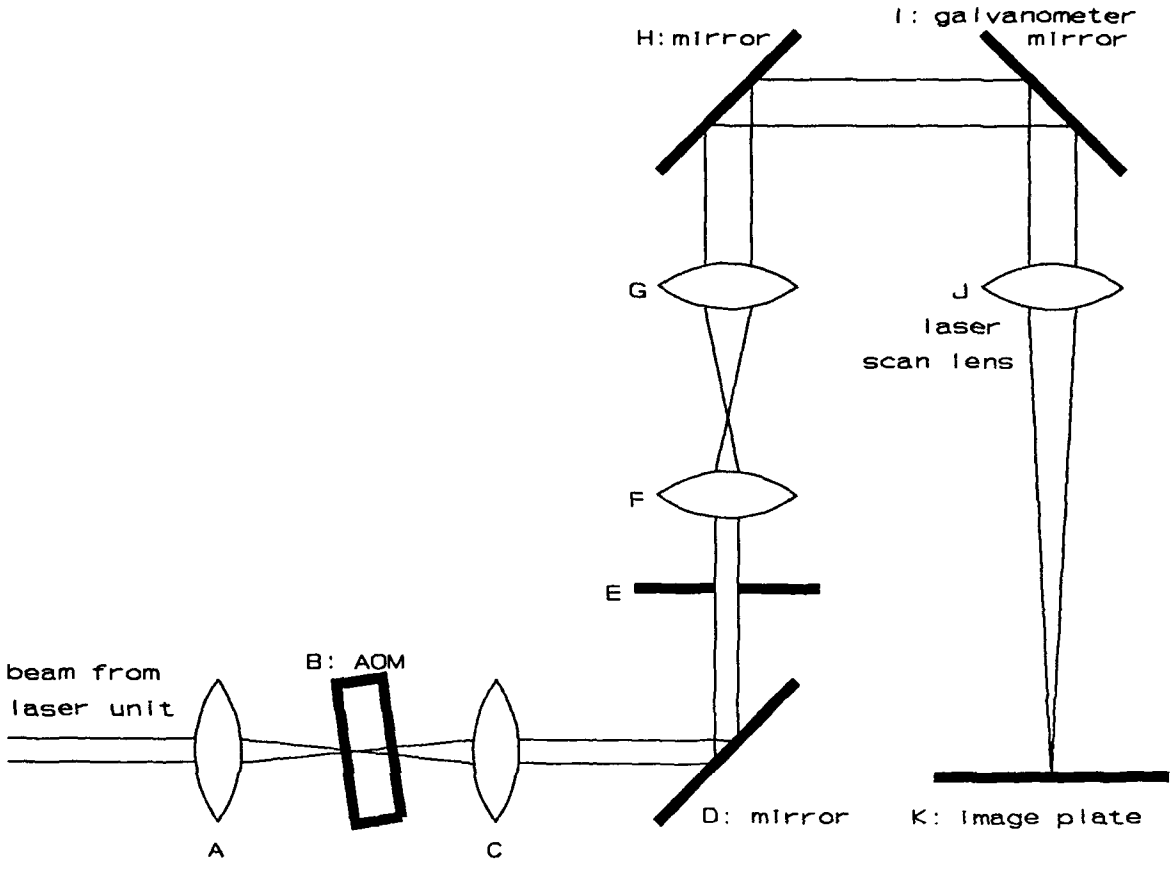

Figure 1 Schematic drawing for the laser scanning optics in an experimental storage phosphor image reader.

The laser spot size at the image plane K, d, is determined by many factors including the focal lengths of the lenses A, E and J. The diameter of the expanded beam at the output of the lens G and the size of the galvanometer mirror I also pose limit on how small the laser spot size can be. We have successfully reduced the laser spot size from 120 μm to 50μm by changing the focal length of lens A from 250mm to 125mm and replacing the lens F (previously a 5x microscopic objective lens) with a 10x one.

Measurement of laser beam spot size

To evaluate the laser spot size, two optical slit-photo Detector assemblies were constructed and attached to one end of the image plate carrier stage. Each assembly consists of a 5μm optical slit and a 2.5mm slit mounted in front of a photo-transistor. The photo transistor output is amplified and then forwarded to an oscilloscope for monitoring. It can also be digitized for analysis in the computer. However, a dedicated high speed analog-to-digital converter would be required to measure sub-millimeter spot sizes with reasonable precision. This option is being planned but not implemented yet.

To measure the laser beam spot size, the assemblies were first positioned in the laser scanning path. As the laser beam scanned across the two optical slits in each assembly, two pulses were generated (Figure 3). The half-maximum width of the two pulses were then measured on the scope. Assuming the (half maximum) pulse widths for the 5μm and 2.5mm slits are t and T respectively, the half maximum width of the laser beam profile on the image plane, d, can be estimated as follows:

$$d = 2.5mm \times \left(\frac{t}{T}\right)$$

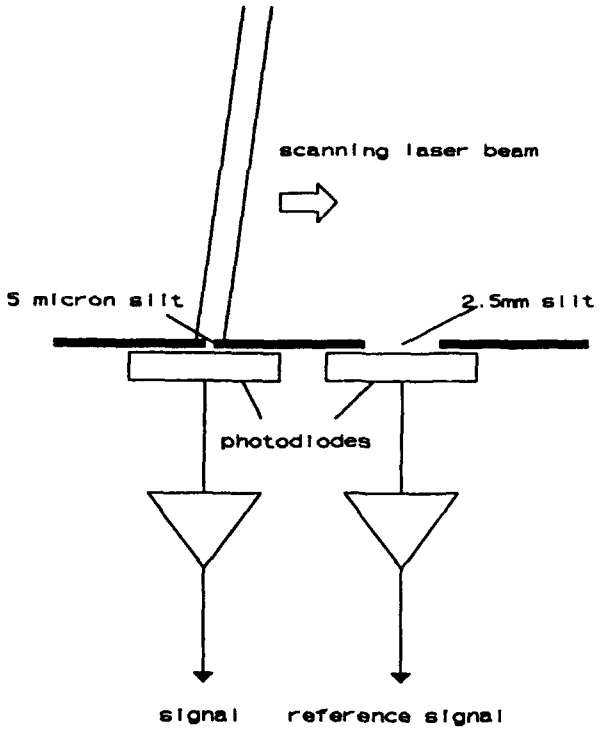

Figure 2 Experimental setup for measuring the laser beam spot size.

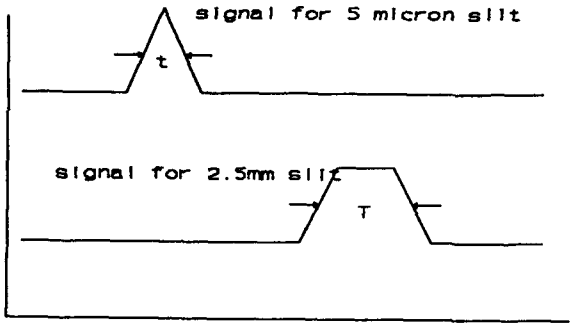

Figure 3 Phototransistor signal outputs for the 5μm and 2.5mm optical slits.

Evaluation of Spatial Resolution Capability

The test pattern used to evaluate the spatial resolution capability is a lead bar resolution pattern (Nuclear Associates 07-553). It consists of 22 groups of bar patterns with a frequency ranging from 0.25 to 10 lps/mm. Each group has a 4 cycle bar pattern. A specification list for the resolution bar pattern is attached as Appendix II.

The bar pattern images are visually examined to evaluate the spatial resolution limit of the imaging system. A fully resolved pattern generally indicates that the MTF is around 0.05 or greater at that particular frequency. A partially resolved pattern indicates that the MTF is probably between 1% and 5%. Unresolved bar patterns generally indicate that the MTF is less than 1%. This observation could vary from person to person but may be used a crude guideline when visually examining the bar pattern images.

Square Wave Response Function, Modulation Transfer Function

The methods for measuring the spatial resolution properties of a storage phosphor imaging system have been previously discussed and demonstrated[8,9,12,13]. Our methods focus on the use a standard resolution test pattern as described before. The square wave response function (SWRF) was measured by plotting the signal profile across the bar patterns and then measuring the average amplitude for each frequency. Because the square waves contain high order harmonics, the SWRF can not be directly used to compute the MTF without correction for these harmonics. We have devised and tested a signal processing method to compute the MTF from the signal profile of a bar pattern.

The signal profile was first segmented into sections of the same frequency. Sections from a number of lines (30-70) were concatenated together into a big array with many more cycles of change. The array was then Fourier transformed and a frequency distribution of the signals was computed. This frequency distribution typically has a fundamental peak followed by a number of high order harmonics. These harmonics generally decrease in magnitude as the order becomes higher. To determine the MTF value, the area under the fundamental peak was computed and normalized by dividing it by the zero frequency component (mean of the data).

Phantom images

Image quality of a mammographic unit is often checked with phantoms simulating a breast with the three major disease symptoms: microcalcifications and masses. Various phantoms have been designed for this purpose. We have used two such phantoms to test the image quality and compare different imaging systems or technical factors. The first one is a Tissue-Equivalent Breast Phantom made by the Computerized Imaging Reference Systems (CIRS), Inc. of Norfolk, Virginia. It consists of a breast shape phantom made of tissue equivalent material, with a step wedge, groups of microcalcifications, masses and fibrils embedded inside the phantom. A specification sheet for the phantom is attached as Appendix III. The step wedge consists a square region with a contrast corresponding to

additional 5mm of glandular tissue over the surrounding background tissue and a second square region with a contrast corresponding to additional 5mm of fat tissue. The 12 microcalcification groups ranges from 0.12mm to 0.35mm in diameter. The 6 masses range from 1mm to 6mm in diameter. The fibrils have a diameter of 8.7μm. This phantom provides a good tool for comparing the overall image quality of different imaging systems, techniques or technical factors.

The second phantom is the RMI Anthropomorphic Breast Phantom (Model 165, Gammex-RMI). The phantom consists of a breast tissue equivalent (50% adipose, 50% glandular) plastic casting and a high resolution detail layer enclosed in a protective acrylic case. Together, these components produce radiographic images that are similar to a true mammogram.. To aid the evaluation of system performance, the phantom also produces a nine level gray scale step wedge and a group of resolution line pairs in the mammogram. The phantom is unique in that the characteristics of its components were derived from an actual mammogram. The three dimensional surface structure of the breast tissue equivalent plastic casting produces the low and medium resolution image detail. High resolution image details are produced by an attenuating coating of a stable mercury-silver amalgam on photographic film. In addition to protecting the contents, the acrylic case acts as a uniform attenuation layer across the entire phantom

When acquiring the storage phosphor images of these phantoms, typical X-ray factors were used. These factors were generally determined by setting the kVp desired and then exposing a Min-R screen-film cassette in the automatic exposure (mAs) mode. The film was then processed and the resulting film image examined to check the density of the image. The kVp and mAs are recorded and used for storage phosphor imaging if the film density appear to be adequate. For the CIRS phantom, the proper techniques for the Min-R screen-film combination are 90 mAs at 28 kVp with an antiscatter used.

Phantom Design and Construction

In the proposed project, we will conduct a ROC study to compare the improved storage phosphor imaging technique with the conventional screen-film technique. The study will be based on images of phantoms with simulated microcalcifications, fibrils and masses. To present more realistic imaging conditions, these objects will be superimposed with structures mimicking tissue structures of breasts. As described by the Statement of work attached as Appendix I, the ROC study will be performed during the third year of the grant period. Image acquisition and printing will be performed during the second year. In the first year of the grant period, we have developed and investigated how to design and construct phantoms for acquiring images to be used in the ROC study. Specifically, we have experimented with methods for simulating microcalcifications, fibrils, masses and overlapping tissue structures. These methods are described and discussed as follows:

Main Body

The main body of phantom provides a background structure over which microcalcifications and masses will be simulated and superimposed. We have investigated several approaches to construct the main body of phantom. Yaffe et al have designed a method which uses a plastic block with a spatially varying thickness generated by numerically controlled milling to simulate tissue structures in a real breast. Clinical mammograms are analyzed and used to compute the thickness variation required to reproduce them. Finer structures, including microcalcifications and low contrast masses, are simulated by an X-ray film of these objects, with the silver atoms chemically replaced by mercury atoms to enhance X-ray attenuation. This approach has been used to produce the mold for mass-producing quality control phantoms (Radiation Measurement Inc.). While the resulting phantoms are reasonably priced and produce realistic images, the original mold is extremely tedious and expensive to make. Since we need 5-10 different phantom patterns in our ROC studies, this approach would be extremely expensive and time consuming.

An alternative approach is to use chunks of muscle tissue embedded in wax to provide various tissue structures. We have used chunks of beef to experiment with this method. Chunks of beef were first placed inside a container with a flat bottom. Melted wax was poured into the container to embed the beef chunks. The phantom was then let to cool and sealed inside a plastic bag. The unused phantoms can be refrigerated for later use. One advantage of this method is the ease of construction. Since the phantom is flat on both the top and bottom sides, it has a uniform thickness, corresponding to a compressed breast. The thickness can be readily controlled by using the right amount of tissue and pouring the wax to a specified height (e.g. 4cm).

Microcalcifications and fibrils

Microcalcifications and fibrils are mainly composed of calcium. Because aluminum has X-ray attenuation properties similar to those of calcium, it has often been used to simulate objects of high calcium contents, e.g. bones and calcifications. To simulate microcalcifications and fibrils, we have acquired and used aluminum wires of several various diameters: 2, 4, 8 and 16 mils (51, 102, 203 and 406μm). These wires were cut into small pieces with the help of a magnifier. To simulate microcalcifications, these wires were cut into pieces with a length significantly shorter than 1mm. Fibrils were simulated by longer pieces, typically with a length of several mm long. Notice that these wire segments were laid down flat on top of the main body of the phantom. Thus, their crosssections are roughly parallel to the X-ray path. Although the wire segments may vary in length, their contrast is predominantly determined by the diameter of their crosssections. Therefore, the locations and diameters of the wire segments will be recorded for each different phantom configuration to provide reference for truth in the ROC studies.

Low contrast masses

Low contrast masses were simulated by wax spheres placed on top of the main body of phantom. In actual imaging situation, the contrast of tumor masses is generated by the difference of X-ray attenuation between the masses and the tissue they replace. Thus, the contrast of a tumor mass is somewhat lower than that of a wax sphere of the same size. To reduce the contrast of the wax spheres, they can be compressed a little bit so that the maximum thickness of the sphere is only a fraction of its diameter.

Quality Control

Quality control of the storage phosphor imaging system has been performed by acquiring and visually checking images of a resolution bar pattern, a CIRS phantom and a RMI anthropomorphic breast phantom. Because many improvements have been made on the system, our criteria for visual check has been updated whenever necessary. However, near the end of the first year, the image quality of the system has somewhat settled down. In general, for the resolution bar pattern image, we expect to see and resolve all bars at frequencies of up to 8.5 lps/mm fully and clearly. The 10 lps/mm bars should be partially resolved. The images of the CIRS phantom provides a convenient semi-quantitative method for checking the overall quality of the system, including the spatial resolution and noise properties. Same technique (28kVp, 90mAs, 65cm SID, with antiscatter grids) will be used in all quality control exposures. In general, we expect to see all microcalcifications with a diameter of 200μm or greater and all masses with a diameter of 3mm or greater. All fibrils should be fully resolved. The RMI phantom offers a more qualitative check. All images should have similar apparent quality as previous images. Because we are planning to further improve the spatial resolution of the system, these criteria will be updated again at the end of first quarter of 1994.

Quality control of mammographic X-ray units and the screen-film combinations have been previously discussed[110,111]. The quality of the mammographic X-ray unit is routinely monitored and maintained by the clinical staff.

Image Data Compression

Two methods were used to develop and implement algorithms for compression of digital mammographic image data. The first method is a lossless scheme which employs image segmentation technique to eliminate data outside the breast area. The second method uses JPEG image data compression algorithm to reduce image data in a lossy fashion. Although this algorithm has been investigated for image data compression in other imaging applications[87], it must be customized for application to mammographic images. This algorithm also results in irreversible change of image data. Therefore, comparison studies will be performed to determine the parameters used in the algorithm. Upon development and optimization of the algorithm, more vigorous comparison studies will be performed to validate the algorithm by ensuring that no significant loss of image quality has been incurred.

RESULTS AND DISCUSSION

System Modification

Based on the above method, we have measured the spot size to be 120μm prior to optics modification and 50μm afterwards. As discussed before, the $1/e^2$ diameter, σ, is often used to describe the beam size in laser optics. σ can be estimated from d as follows:

$$\sigma = \sqrt{\frac{2}{\ln 2}} \cdot d$$

Thus, with our recent modification of the laser scanning optics, the $1/e^2$ diameter, has been reduced from 204μm to 85μm. From a theoretical point of view, a further reduction of the $1/e^2$ diameter from 85μm to 50μm would still result in a significant improvement of the resolution capability of the system. This corresponds to a reduction of the half maximum width from 50μm to about 30μm. At the beginning of the second year of the grant period, we will attempt to further reduce the beam spot size and determine the smallest beam spot size that can be practically achieved and can improve the overall system resolution.

To further reduce the beam spot size, we plan to replace the AOM(Acoustic-Optical Modulator) with a more efficient one and move it to between the laser unit and Lens A. This is possible because the new AOM does not required focused beam and can operate on direct output from the laser unit. A small aperture (10-30μm in diameter) will be positioned at the focal point between Lens A and Lens C. The use of this aperture will force the beam spot size to be reduced throughout the rest of the optics. However, a significant amount of laser power will be sacrificed through blocking the light outside the aperture.

Another source for loss of laser power is through the beam expander G, galvanometer mirror I and laser scan lens J. During our first stage of system modification, adequate but marginal laser power was achieved with currently used beam expander, galvanometer mirror and laser scan lens. However, they could limit the laser power to unusable range if further reduction of the beam spot size (down to 25-30μm) is desired. Instead of replacing these components, a easier approach is to use a more efficient AOM (Multiwavelength Visible Light Modulator, Model No. N48062-2.5-.55, NEOS Technologies Inc.) and increase the power available at the beginning. The new AOM has a maximum light transmission of over 90% and therefore can produce a much higher power than the previously used one (made by Newport Research Inc., with an efficiency of less than 10%). This higher power provides us a greater flexibility in further reducing the beam spot size. The replacement of the AOM is currently undergoing and expected to be completed by end of 1993.

Another side effect of reducing the spot size is the substantially increased aliasing effects which occurs when the small spot size is used in conjunction with large sampling distances, e.g. 86 or 172μm used in chest imaging. To resolve this problem and to allow us perform a more detailed study on the effects of beam spot sizes, we will implement a mechanism to vary the beam spot size through computer control. The current plan is to mount the microscopic objective lens F on a micro-translational stage and move it slightly along the optical axis to focus (make the spot size smaller) or defocus (make the spot size larger) the light beam between Lens F and Lens G.

Resolution Bar Pattern Images

Films 1 and 2 shows two images of the resolution bar pattern obtained with the improved storage phosphor imaging system. The bar patterns are oriented in horizontal and vertical directions in Film 1 and at 45 degrees in Film 2. Notice that in all images all bars with a frequency of 8.5 lps/mm or lower are fully and clearly resolved. Upon careful examination, the 10 lps/mm bars are only partially resolved.

Film 3 shows an image of the resolution bar pattern obtained with the unmodified storage phosphor imaging system. Notice that, although also scanned with a pixel size of 43μm, it can only resolve 5 lps/mm while the modified imaging system resulted in clearly resolved bar patterns at up to 8.5 lps/mm.

Film 4 shows an image of the resolution bar pattern obtained with a Min-R screen-film combination. Notice that the 10 lps/mm bars can be resolved slightly better than in the storage phosphor image. The image of the bar patterns has a slightly sharper appearance than the storage phosphor image. However, the resolution quality of the storage phosphor image is rather close to that of the screen-film images.

Figure 4 shows the Square Wave Response Function (SWRF) measured from the bar pattern image in Film 1. Notice that these data agree with our observation of the resolution bar images. At 10 lps/mm, the SWRF is 2-3% while the bars are partially resolved in the image. At 8.5 lps/mm or lower frequencies, the SWRF is 5% or greater while all bars are fully resolved.

We have also used the Fourier filtering method to compute the MTF from the bar pattern signals. This has resulted in reasonable measurements. However, we have found the results have some fluctuation and do not appear as stable as the SWRF at frequencies lower than 2 lps/mm. Currently, we are still trying to understand this phenomenon and to devise a method to normalize the measurements so that the extrapolated MTF value at zero frequency would be 1.

Phantom images

The CIRS phantom has been used to compare the spatial resolution capability of the improved imaging system with those of the unmodified system and conventional screen-film combinations.

Film 5 shows an image of the CIRS phantom acquired with the modified imaging system. Film 6 shows an image of the CIRS phantom acquired with the unmodified imaging system. Film 7 shows an image of the CIRS phantom acquired with a Min-R screen-film combination. Notice that in the screen-film image, all microcalcifications with a diameter of 200μm or greater, all masses with a diameter of 3mm or greater and all fibrils are resolved. All these components are resolved in the storage phosphor image acquired with the modified system, too. This indicates that the image quality from the modified storage phosphor imaging system approaches that of a conventional screen-film combination. However, the storage phosphor image can be digitally enhanced. Therefore, it can be displayed or printed with higher contrast to enhance low contrast details over various parts of the image. It can also be displayed with larger dynamic range to show the skin line more clearly.

The storage phosphor image acquired with the unmodified system shows a much worse quality. Fewer groups of microcalcifications, masses and fibrils can be seen in the image. This clearly demonstrates the improvement of the image quality resulted from reducing the beam spot size.

Film 8 shows an image of the RMI phantom acquired with the modified storage phosphor imaging system. Film 9 shows an image of the RMI phantom acquired with an Min-R screen-film system. Notice that although the screen-film image is slightly sharper the two images show about the same amount of details. Due to the window and level setting, the storage phosphor image shows higher contrast.

It should noted that the phantom images presented here have some artifacts, including bright dots from dust and horizontal structures resulting from the unstable AOM. These artifacts can be eliminated by carefully cleaning the storage phosphor screens and using a new improved AOM (see the System Modification sections). The artifacts will be carefully monitored and eliminated during actual image acquisition for the ROC studies.

Phantom Design and Construction

We have constructed several phantoms by using chunks of beef embedded in wax to see if proper images could be made for the ROC studies. Sub millimeter segments of aluminum wires were placed on top of the phantom to simulate microcalcifications. Two images of a phantom constructed using the above described method are shown by Films 10 and 11. Film 10 is a storage phosphor image acquired with a commercial prototype

image reader (KESPR, Eastman Kodak Co.) and a 8"x10" high resolution screen. Film 11 is a screen-film image acquired with a clinical mammographic unit at our institution. Notice that although the phantom images do not exactly mimic a mammogram, they do provide adequate variation of tissue structures as background for detection of the microcalcifications and other details simulated.

Data Compression

The image compression study consists of three major tasks: (1) develop and test lossless compression algorithms, (2) develop and test lossy compression algorithms and (3) evaluate the compression algorithms through JND (Just Noticeable Difference) studies.

In our first year of the grant period, we have completed most of the first two tasks. We have developed and tested both lossless and lossy compression algorithms. They have been successfully used for data compression of digital mammograms. We are currently evaluating image noises in different regions inside and outside the breast area to assess ways to optimize the compression ratio with minimum degradation of image quality. Upon completion of tests, we will perform our first JND (Just Noticeable Difference) study to evaluate the detectability of differences between compressed and non-compressed digital mammograms as perceived by radiologists and image processing specialists.

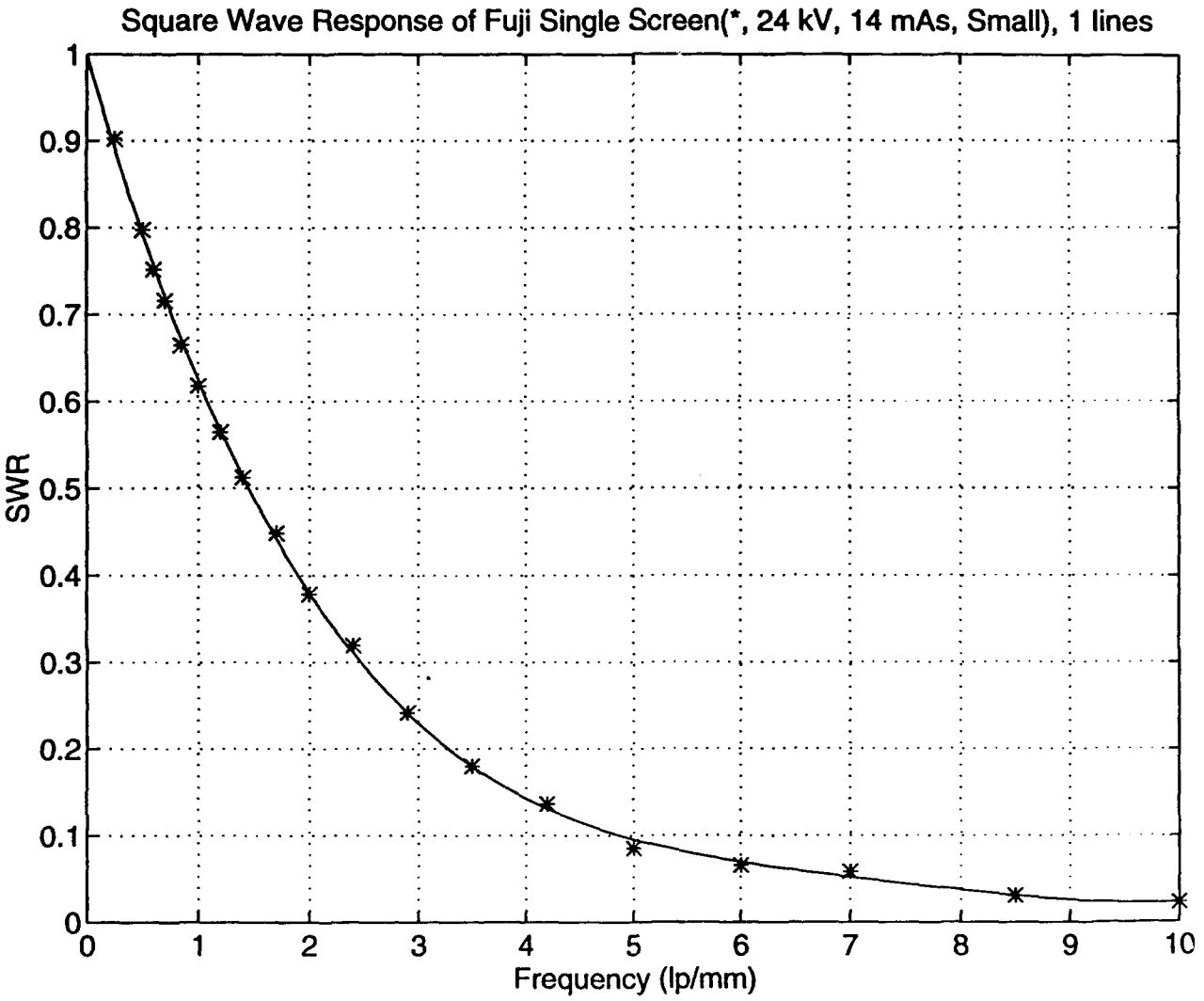

Figure 4 Square Wave Response Function (SWRF) for the modified storage phosphor imaging system with a beam spot size reduced from 120μm to 50μm.

CONCLUSIONS

To summary our accomplishment in the first year of the grant period:

1. We have successfully modified our storage phosphor image reader and reduced the laser beam spot size from 100μm to 50μm.

2. The reduction of the laser beam spot size resulted in a significant improvement of the spatial resolution capability of the storage phosphor imaging system. This improvement allows us to easily resolve 8.5 lps/mm bar patterns at 28 kVp on a mammographic unit.

3. Using a breast phantom for comparison, the quality of the storage phosphor images, obtained with the improved imaging system, is comparable to that of the screen-film images acquired with a clinical mammographic unit at our institution.

4. We plan to implement the capability to vary the spot size through computer control. We plan to further reduce the spot size and test to see if further improvement is possible and whether we have reached the optimal spot size. Following these studies, we will start acquiring phantom images for the ROC studies.

The completion of these tasks has resulted in a storage phosphor imaging system with a spatial resolution capability approaching that of conventional screen-film combinations for mammographic applications. In the first quarter of 1994, we will attempt to further reduce the beam spot size and optimize the system performance. Upon completion of this further system modification, we will be largely prepared to start acquiring images for the ROC studies.

REFERENCES*

1. Fuhrman CR, Gur D, Good BC, et al. The diagnostic quality of storage phosphor radiographs compared to conventional films: interpreter's perception. AJR 1988; 150:1011-14.
2. Fuhrman CR, Gur D, Schaetzing R. High resolution digital imaging with storage phosphors. J Thoracic imaging 1990; 5:12-30.
3. Gur D, Deutsch M, Fuhrman CR, et al. The use of storage phosphors for portal imaging in radiation therapy: therapists's perception of image quality. Med Phys 1989; 16(1):132-6.
4. Weiser JC, Gur D, Cano E, Deutsch M, Wu A, Mogus R. Verification of electron beam therapy with storage phosphor images: precision of field placement. Radiol 1990; 175:257-259.
5. Slasky BS, Gur D, Good WF, Costa-Greco MA, Harris KM, Cooperstein LA, Rockette HE. Receiver operating characteristic analysis of chest image interpretation with conventional, laser-printed, and high-resolution workstation images. Radiol 1990; 174:775-780.
6. Rosenthal MS, Good WF, Costa-Greco MA, Miketic LM, Eelkema EA, Gur D, Rockette HE. The effect of image processing on chest radiograph interpretations in a PACS implementations in a PACS environment. Invest Radiol 1990; 25:897-901.
7. Schaetzing R, Whiting BR, Lubinsky AR, Owen JF. Digital radiography using storage phosphors. in Digital imaging in diagnostic radiology, published by Churchil Livingstone (1989).
8. Hillen W, Schievel U, Zaengel T. Imaging performance of a digital storage phosphor system. Med Phys 1987;14:744.
9. Fujita H, Ueda K, Morishita J, Fujikawa T, Ohtsuka A, Sai T. Basic imaging properties of a computed radiographic system with photostimulable phosphors. Med Phys 1989;16(1):338-345.
10. Lubinsky AR, Owen JF, Korn DM. Storage phosphor system for computed radiography: screen optics. SPIE 1986;626:120-132.
11. Lubinsky AR, Whiting BR, Owen JF. Storage phosphor system for computed radiography: optical effects and detective quantum efficiency (DQE). SPIE 1987;767:167-177.
12. Fujita H, Ueda K, Ohtsuka A. Resolution property of digital radiography with photostimulable phosphors. I. Measurements of imaging plate MTF's. Jpn J Med Imag Inform Sooc 1987; 4:89.
13. Fujita H, Ueda K, Fujikawa, Ohtsuka A. Resolution property of digital radiography with photostimulable phosphors. II. Measurements of digital characteristic curve and presampling MTF. Jpn J Med Imag Inform Sooc 1988; 5:1.
14. Shaw CC, Herron JM, Gur D. Signal fading, erasure and rescan in storage phosphor imaging. SPIE 1992;1651 Image Physics. In press.
15. Bunch PC. Dectective quantum efficiency of selected mammographic screen-film combinations. Proc SPIE 1989; 1090:67-77.
16. Silverberg E, Lubera JA: A Review of American Cancer Society estimates of cancer cases and deaths. CA 1983; 33:2-8.
17. Silverberg E: Cancer statistics, 1983. Ca 1983; 33:9-25.
18. Nathan S: An Atlas of Normal and Abnormal Mammograms. Oxford; New York; Oxford University Press, 1982.

19. Feig SA, McLelland R, Eds: Breast Carcinoma: Current Diagnosis and Treatment. New York, Masson Publishing USA, Inc, and the American College of Radiology, Chicago, 1983.
20. National Task Force on Breast Cancer Control: Mammography: A statement of the American Cancer Society. Conn Med 1983; 47:37-9.
21. Moskowitz M, Gartside PS: Evidence of breast cancer mortality reduction: Aggressive screening in women under age 50. AJR 1982; 138:911-6.
22. Venet L, Shapiro S, Strax P, Venet W: Effect of screening on survivals. In: Early Breast Cancer/Detection and Treatment, New York, John Wiley & Sons, 1975.
23. Pavlov KA, Semiglazov VF: Detection of early forms of breast cancer by mass screening examinations. Neoplasma 1981; 28:611-5.
24. Breast Cancer Digest 1979; 80:1691.
25. Strax P: Control of breast cancer through mass screening. JAMA 1976; 235:1600-2.
26. Thomas BA, Price JL, Boulter PS. Breast cancer population screening by single view mammography with selective clinical examination--A pilot study. Clin Oncol 1981; 7:201-4.
27. Tabar L, Gad A: Screening for breast cancer: The Swedish trial. Radiology 1981; 138:219-22.
28. Andersson I, Andren L, Hildell J, Linell F, Ljungqvist U, Pettersson H: Breast cancer screening with mammography. Radiology 1979;273-6.
29. Beahrs OH, Shapiro S, Smart C: Report of the working group to review the NCI/ACS breast cancer detection demonstration projects. NCI 1977.
30. Beahrs OH, Shapiro S, Smart CH, et al: Report of working group to review BCDDP. J Natl Cancer Inst 1979; 62:679-90.
31. Strax P: Organization of mass screening programs in breast cancer--Including identification of high-risk groups. In: Early Diagnosis of Breast Cancer, Grundman E, Beck L, Eds. Stuttgart, Gustav Fischer Verlag, 1978.
32. Lundgren B, Helleberg A: Single oblique-view mammography for periodic screening for breast cancer in women. JNCI 1982; 68:351-5.
33. Haus AG: Physical principles and radiation dose in mammography. Med Radiogr Photogr 1982; 58:70-80.
34. Moskowitz M, Gartside PS, Gardella L, deGroot I, Guenther D: The breast cancer screening controversy: A perspective. In: Breast Carcinoma: The Radiologist's Expanded Role. Logan WW, Ed. New York, John Wiley & Sons, 1977, pp 3[illegible]-52.
35. Moskowitz M: Screening for breast cancer: How effective are our tests? A critical review. CA 1983; 33:26-39.
36. Moskowitz M: Mammographic screening: Significance of minimal breast cancers. AJR 1981; 136:735-8.
37. Leborgne RA: The Breast in Roentgen Diagnosis. London, Constable and Co., 1953.
38. Ingleby H, Gershon-Cohen J: Comparative Anatomy, Pathology and Roentgenology of the Breast. Philadelphia, University of Pennsylvania Press, 1960.
39. Stanton L, Villafana T, Day JL, Lightfoot DA: A breast phantom method for evaluating mammography technique. Invest Radiol 1978; 13:291-7.
40. Miller DW: Center for Radiological Physics: Mammography Review Procedures and Results. In: Breast Carcinoma: The Radiologist's Expanded Role. Logan WW, Ed. New York, John Wiley & Sons, 1977, pp 129-33.
41 Porrath SA: XERG mammography: A review of sixteen months experience plus a comparison with xeromammography. In: Logan W, Muntz EP, Reduced Dose Mammography. New York, Masson Publishing USA, 1979, pp 389-94.

42. Hirschfeld RL: XERG and lo-dose mammography: A comparative clinical study. In: Logan WW, Muntz EP: Reduced Dose Mammography. New York, Masson Publishing USA, 1979, pp 395-405.
43. Sickles EA: Heavy-particle mammography. In: Breast Carcinoma: The Radiologist's Expanded Role. Logan WW, Ed. New York, John Wiley & Sons, 1977, pp 239-41.
44. Isard HJ: General discussion: Thermography in the mass screening of cancer. Ann NY Acad Sci 1980; 335:520-3.
45. Milbrath JR: Does thermography aid in breast cancer detection? In: Breast Carcinoma: The Radiologist's Expanded Role. Logan WW, Ed. New York, John Wiley & Sons, 1977, pp 255-8.
46. Chang CHJ, Sibala JL, Fritz SL, Dwyer SJ III, Templeton AW: Specific value of computed tomographic breast scanner (CT/M) in diagnosis of breast diseases. Radiology 1979; 132:647-52.
47. Gisvold JJ,Karsell PR, Reese DF: Computerized tomographic mammography. In: Breast Carcinoma: The Radiologist's Expanded Role. Logan WW, Ed. New York, John Wiley & Sons, 1977, pp219-38.
48. Bryan RN, Hazelwood CF, Ford JJ, Fisher PB, Schneiders NJ, Garnil E: In vivo NMR imaging of the human breast. Presented at the 69th Annual Meeting of the Radiological Society of North America, Chicago, 1983.
49. Sickles EA, Davis PL, Crooks LE: NMR characteristics of benign and o84 malignant breast tissues: Preliminary report. Presented at the 69th Annual Meeting of the Radiological Society of North America, Chicago, November 1983.
50. El-Yousef SJ, O'Connell DM, Duchesneau RH, et al. Radiofrequency pulse sequences for characterization of benign and malignant conditions of the breast. Radiology 1984; 153:52.
51. Cole-Beuglet C, Baltarowich O, Pasto ME, Rifkin MD, Kurtz AB, Goldberg BB: Ultrasound appearance of carcinoma in younger patients. Presented at the 69th Annual Meeting of the Radiological Society of North America, Chicago, November 1983.
52. McSweeney MB, Egan RL: Solid breast masses: Ultrasonographic, mammographic, and pathologic correlation. Presented at the 69th Annual Meeting of the Radiological Society of North America, Chicago, November 1983.
53. Muntz EP, Wilkinson E, George FW: Mammography at reduced doses: Present performance and future possibilities. AJR 1980; 134:741-7.
54. Jennings RJ, Eastgate RJ, Siedband MP, Ergun DL: Optimal x-ray spectra for screen-film mammography. Med Phys 1981; 8:629-39.
55. Brodie I, Gutcheck RA: Radiographic information theory: Correction for x-ray spectral distribution. Med Phys 1983;10:293-300.
56. Barnes GT, Chakraborty DP: Radiographic mottle and patient exposure in mammography. Radiology 1982; 145:815-21.
57. Egan RL, McSweeney MB, Sprawls P: Grids in mammography. Radiology 1983; 146:359-62.
58. Barnes GT: Radiographic mottle: A comprehensive theory. Med Phys 1982; 9:956-67.
59 Zarand P, Pentek: Absorbed dose in "high filtration" xeromammography--An intercom parison. Radiol Diagn 1981; 22:240-6.
60. Sickles EA: Mammographic detectability of breast micro- calcifications. AJR 1982; 139:913-8.
61. Haus AG: Effect of geometric unsharpness in mammography and breast xeroradiography. In:Breast Carcinoma: The Radiologist's Expanded Role. Logan WW, Ed. New York, John Wiley & Sons, 1977, pp 93-108.

62. Brodie I, Gutcheck RA: Radiographic information theory and application to mammography. Med Phys 1982; 9:79-95.
63. Dodd GD: Radiation detection and diagnosis of breast cancer. Cancer 1981; 47:1766-9.
64. Hammerstein GR, Miller DW, White DR, Masterson ME, Woodard HQ, Laughlin JS: Absorbed radiation dose in mammography. Radiology 1979; 130:485-91.
65. Haus AG. Technologic improvements in screen-film mammography. Radiology 1990; 1174:628-37.
66. Haus AG. Recent trends in screen-film mammography: technical factors and radiation dose. Recent Results Cancer Res 1987; 105:37-51.
67. Haus AG. Recent advances in screen-film mammography. Radiol Clin north Am 1987; 25:913-28.
68. Sickles EA: Mammographic detectability of breast microcalcifications. AJR 1982; 139:913-8.
69. Muir BB, Lamb J, Anderson TJ, Kirkpatrick AE: Microcalcification and its relationship to cancer of the breast: Experience in a screening clinic. Clin Radiol 1983; 34:193-200.
70. Chan HP, Vybomy CJ, MacMahon H, Metz CE, Doi K, Sickles EA. Digital mammography: ROC studies of the effects of pixel size and unsharp-mask filtering on the detection of subtle microcalcifications. Invest Radiol 1987; 22:581-9.
71. Chan HP, Doi K, Galhotra S, Vybomy CJ, MacMahon H, Jokich PM. Image feature analysis and computer-aided diagnosis in digital radiography. I. Automated detection of microcalcifications in mammography. Med Phys 1987; 14:538-48.
72. Belikova TP, Yaroslavsky LP. Comments on "Image feature analysis and computer-aided diagnosis in digital radiography. I. Automated detection of microcalcifications in mammography." letter to Med Phys 1989; 16:142.
73. Chan HP, Doi K, Vybomy CJ, Schmidt RA, Metz CE, Lam KL, Ogura T, Wu Yz, MacMahon H. Improvement in radiologists' detection of clustered microcalcifications on mammograms: the potential of computer-aided diagnosis. Invest Radiol 1990; 25:1102-10.
74. Fam BW, Olson SL, Winter PF, Scholz FJ. Algorithm for the detection of fine clusttered calcifications on film mammograms. Radiology 1988; 169:333-7.
75. Dhawan AP, Le Royer E. Mammographic feature enhancement by computerized image processing. Comput Methods Programs Biomed 1988; 27:23-35.
76. Davies DH, Dance DR. Automatic computer detection of clustered calcifications in digital mammograms. Phys Med Biol 1990; 35:1111-8.
77. Fujita H, Ueda K, Ohtsuka A. Resolution property of digital radiography with photostimulable phosphors. I. Measurements of imaging plate MTF's. Jpn J Med Imag Inform Sooc 1987; 4:89.
78. Fujita H, Ueda K, Fujikawa, Ohtsuka A. Resolution property of digital radiography with photostimulable phosphors. II. Measurements of digital characteristic curve and presampling MTF. Jpn J Med Imag Inform Sooc 1988; 5:1.
79. Barnes GT, Sones RA, Tesic MM. Digital chest radiography: performance evaluation of a prototype unit. Radiology 1985; 154:801-806
80. Doi K, Fujita H, Ohara K, et al. Digital readiographic imaging system with multiple slit scanning x-ray beam: preliminary report. Radiology 1986; 161:513-518.
81. Templeton AW, Dwyer III SJ, Cox GG, et al. A digital radiology imaging system: description and clinical evaluation. AJR 1987; 149:847-851.
82. Slasky BS, Sashin D, et al. Digital radiography of the chest by self-scanning linear diode arrays. Acta Radop;pgica 1987; 28:461-466.
83. Fritz SL, Chang CH, Gupta NK, Martin NL, Laws RL, Anderson WH, Dwyer SJ, Templeton AW, Bernardi R, Fox T. A digital radiographic imaging system for mammography. Invest Radiol 1986; 21:581-3.

84. Rosenthal MS, Sashin D, Herron J, Maitz G, Boyer J, Gur D. Evaluation of a moving slit technique for mammography. SPIE 1991;1443 Medical Imaging V-Image Physics:132-142.
85. Nishikawa RM, Mawdsley GE, Fenster A, Yaffe MJ. Scanned-projection digital mammography. Med Phys 1987; 14:717-27.
86. Holdsworth DW, Gerson RK, Fenster A. A time-delay integration charge-coupled device camera for slot-scanned digital radiography. Med Phys 1990; 17:876-86.
87. Good WF. Bit allocation tables for the compression of chest images by JPEG type algorithms. SPIE 1992;1652 Image Processing. In press.
88. Photometrics. Charge-coupled devices for quantitative electronic imaging. 1991. Tuscon: Photometrics Ltd. 1-28.
89. Kennedy WH, Herron JM, Gur D, et al. X-ray imaging with two-dimensional CCD arrays. Med Phys 1985; 12(4):504.
90. Herron JM, Gur D, Daxon EG, Good WF, Shaw CC, et al. Digital x-ray imaging with two-dimensional charge-coupled device (CCD) arrays. Proc SPIE 1990; 1231:472-478.
91. Lawrence JL, Cope AD, Herron JM, et al. Medical x-ray imaging applications of the TEK2048 CCD. Proc SPIE 1990; 1242:59-65.
92. Kimme-Smith C, Bassett LW, Gold RH, Gormley L. Digital mammography: a comparison of two digitization methods. Invest Radiol 1989; 24:869-75.
93. Oestmann JW, Kopans D, Hall DA, McCarthy KA, Rubens JR, Greene R. A comparison of digitized storage phosphors and conventional mammography in the detection of malignant microcalcifications. Invest Radiol 1988; 23:725-8.
94. Kato Hisatoyo. Photostimulable phosphor radiography: design considerations. Proc AAPM Summer School: Specification, Acceptance Testing and Quality Control of Diagnostic X-ray Imaging Equipment 1991.
95. Melles Griot Optics guide. Vol. 5, Chapters 17-21, 1991.
96. Stanton L, Day JL, Villafana T, Miller CH, Lightfoot DA. Screen-film mammographic technique for breast cancer screening. Radiology 1987; 163:4771-9.
97. Goodman LR, et al. Digital and conventional chest images:observer performance with film digital radiography system. Radiology 1986; 158:27-33.
98. Hanley JA, McNeil BJ. The meaning and the use of the area under a receiver operating characteristic (ROC) curve. Radiol 1982; 143:29-36.
99. Hanley JA, McNeil BJ. A method of comparing the areas under receiver operating characteristic curves derived from the same cases. Radiol 1983; 148:839-843.
100. Kelsey CA, Mettler FA. ROC analysis can reveal best diagnostic method. Diagnost Imag 1989; 155-161.
101. McNeil BJ, Hanley JA. Statistical approaches to the analysis of receiver operating characteristic (ROC) curves. Med Decis Making 1984; 4:137-150.
102. Metz CE. ROC methodology in radiologic imaging. Invest Radiol 1986; 21:720-733.
103. Swets JA. ROC analysis applied to the evaluation of medical imaging techniques. Invest Radiol 1979; 14:109-121.
104. Swets JA, Pickett RM. Evaluation of diagnostic systems: methods from signal detection theory. New York: Academic Press 1982.
105. Rockette HE, Gur D, Cooperstein LA, Obuchowski NA, King JL, Fuhrman CR, Tabor EK, Metz CE. Effect of two rating formats in multi-disease ROC study of chest images. Invest Radiol 1990;25:225-29.
106. Gur D, Rockette HE, Good WF, Slasky BS, Cooperstein LA, Straub WH, Obuchowski NA, Metz CE. Effect of observer instruction on ROC study of chest images. Invest Radiol 1990;25:230-34.

107. Rockette HE, Obuchowski NA, Gur D. Non-parametric estimation of degenerate ROC data sets used for comparison of imaging systems. Invest Radiol 1990;25:835-37.
108. Rockette HE, Gur D, Metz CE. The use of continuous and discrete confidence judgments in Receiver Operating Characteristic studies of diagnostic imaging techniques. Invest Radiol 1992;27:169-172.
109. Caldwell CB, Yaffe MJ, "Development of an anthropomorphic breast phantom", Med Phys 1990; 17(2): .
110. Screen film mammography: Imaging considerations and medical physics responsibilities, Ed. by Gary Barnes and G. Donald Frey, Medical Physics Press, Madison, WI, 1991.
111. AAPM Report No. 29: Equipment requirement and quality control for mammography, Ed. by M. J. Yaffe et al, Published for the American Association of Physicists in Medicine by the American Institute of Physics.

* *For convenience, this reference list was adopted from the original proposal. However, the list has been updated and several new references were added. It should be noted that not all references are cited in this report.*

APPENDIX I

SPECIFICATIONS FOR THE RESOLUTION TEST PATTERN
(Nuclear Associates, Model 07-553)

Figure 1 is an enlarged contact radiograph of the test plate. The spacing of the bar pattern varies in steps between the index marks. For example, the spatial frequency of the pattern between AB is one-half line pair per millimeter and the spatial frequency between CD is 0.85 line pairs per millimeter.

Table #1 tabulates the spatial frequency associated with each of the index marks. A larger line separates the pattern into a group of line pairs with longer lines corresponding to groups of 0.5, 1, 2, 5 and 10 line pairs per millimeter.

Fig. 1

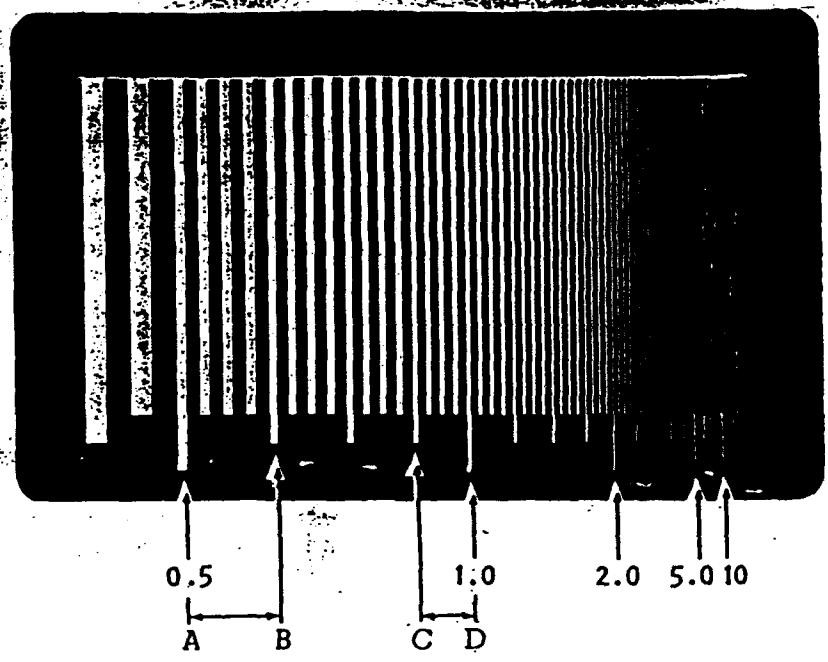

Table #1 The line pairs/mm value for each resolution group is listed below.

Group	LP/mm							
1	0.25	7	1.2	13	3.5	19	10
2	0.5	8	1.4	14	4.2	20	8.5
3	0.6	9	1.7	15	5.0	21	7
4	0.7	10	2.0	16	6	22	6
5	0.85	11	2.4	17	7		
6	1.0	12	2.9	18	8.5		

APPENDIX II

SPECIFICATIONS FOR THE CIRS BREAST PHANTOM
(Computerized Imaging Reference Systems, Inc.)

Map of Embedded Details in Phantoms.

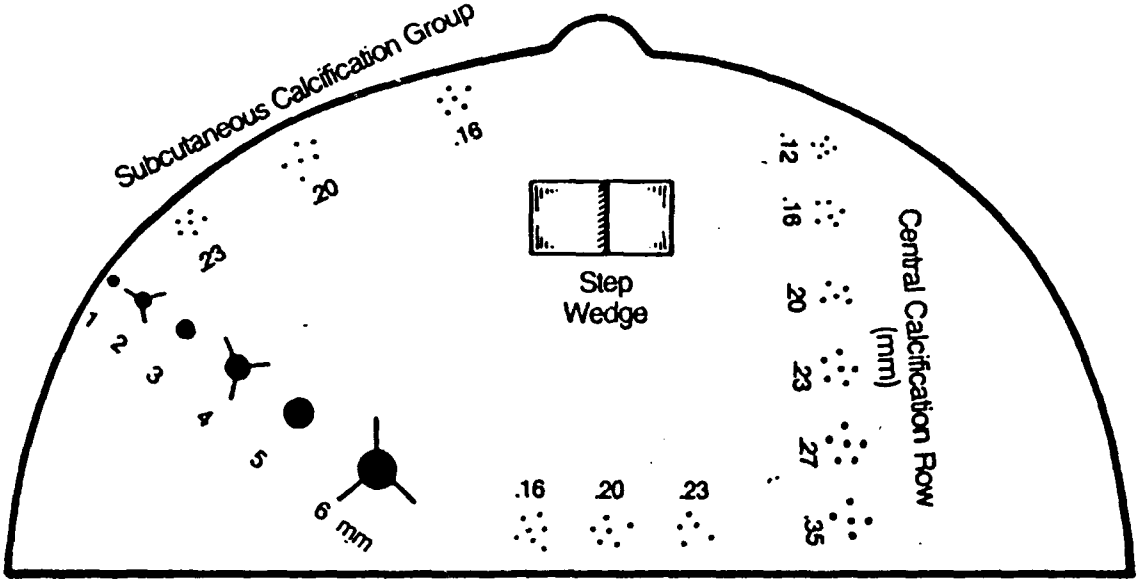

- **Stepwedge**
  5 mm glandular equivalent/5 mm fat equivalent
- **Microcalcifications ($CaCO_3$)**
  12 groupings with largest at .35 mm diameter and smallest at .12 mm diameter. This range of sizes has been shown in practice to be sensitive to system calibration and performance.
- **Masses**
  6 simulated tumor masses ranging from 6 mm diameter to 1 mm diameter
- **Fibrils**
  3 fibre spiculations

CIRS COMPUTERIZED IMAGING REFERENCE SYSTEMS, INC.
2488 Almeda Avenue, Norfolk, Virginia 23513
Tel: (804) 855-2765

APPENDIX III

SPECIFICATIONS FOR THE ANTHROPOMORPHIC BREAST PHANTOM
(Model 165, Gammex-Radiation Measurement Inc.)

Specifications

Breast Tissue Equivalent Plastic Casting	Tissue Equivalent Plastic, RMI Model 454 50% adipose, 50% glandular, (BR-12 equivalent)
High Resolution Layer	*Radiographic film containing a stable mercury-silver amalgam.* 9 step gray level stepwedge. Resolution Bar Pattern: 5–25 lp/mm
Phantom Case	Case Material: Acrylic Top Thickness: 0.215 in Bottom Thickness: 0.175 in
Overall Dimensions	19.6 x 11.7 x 6.1 cm (7.7 x 4.7 x 2.4 in) 0.7 kg (1.6 lb)

Note: Due to our philosophy of continuous product improvement, these specifications may change without notice.

7

CAPTIONS FOR FILMS - Cannot be reproduced

Film 1 Storage phosphor image of two resolution test patterns (oriented horizontally and vertically respectively) acquired with the modified storage phosphor image reader with a reduced beam spot size of 50μm.

Film 2 Storage phosphor image of a resolution test pattern (tilted at 45 degrees) acquired with the modified storage phosphor image reader with a reduced beam spot size of 50μm.

Film 3 Storage phosphor image of a resolution test patterns acquired with the unmodified storage phosphor image reader with a beam spot size of 120μm.

Film 4 Image of two resolution test patterns (oriented horizontally and vertically respectively) acquired with a Min-R screen-film combination.

Film 5 Storage phosphor image of a CIRS breast phantom acquired with the modified storage phosphor image reader with a reduced beam spot size of 50μm.

Film 6 Storage phosphor image of a CIRS breast phantom acquired with the unmodified storage phosphor image reader with a beam spot size of 120μm.

Film 7 Image of a CIRS breast phantom acquired with a Min-R screen-film combination.

Film 8 Storage phosphor image of a RMI breast phantom acquired with the modified storage phosphor image reader with a reduced beam spot size of 50μm.

Film 9 Image of a RMI breast phantom acquired with a Min-R screen-film combination.

Film 10 Storage phosphor image of the experimental phantom acquired with a commercial storage phosphor image reader (Kodak Ektascan Storage Phosphor Image Reader).

Film 11 Image of the experimental phantom acquired with a Min-R screen-film combination.